Article

Quantitative Structure#Activity Relationships for Aqueous Metal#Siderophore Complexes

Owen W. Duckworth, John R. Bargar, and Garrison Sposito

Environ. Sci. Technol., **2009**, 43 (2), 343-349• DOI: 10.1021/es802044y • Publication Date (Web): 10 December 2008

Environ. Sci. Technol. **2009,** *43,* 343–349

Quantitative Structure−Activity Relationships for Aqueous Metal−Siderophore Complexes

OWEN W. DUCKWORTH,*,† JOHN R. BARGAR,‡ AND GARRISON SPOSITO§

Department of Soil Science, North Carolina State University, Raleigh, North Carolina 27695-7619, Stanford Synchrotron Radiation Lightsource 2575 Sand Hill Road, Building 137, MS 69, Menlo Park, California 94025, and Division of Ecosystem Sciences, University of California, Berkeley, California 94720-3114

Received July 23, 2008. Revised manuscript received October 20, 2008. Accepted October 29, 2008.

Siderophores, biogenic chelating agents that facilitate the solubilization and uptake of ferric iron, form stable complexes with a wide range of nutrient and contaminant metals and thus may profoundly affect their fate, transport, and biogeochemical cycling. To understand more comprehensively the factors that control the stability and reactivity, as well as the potential for microbial uptake, of metal−siderophore complexes, we probed the structures of complexes formed between the trihydroxamate siderophore desferrioxamine B (DFOB) and Cu(II), Ga(III), Mn(II), Ni(II), and Zn(II) in solution by using extended X-ray absorption fine structure (EXAFS) spectroscopy. We find that all metals studied are dominantly in octahedral coordination, with significant Jahn−Teller distortion of the Cu(II)HDFOB^0 complex. Additionally, log-transformed complex stability constants correlate not only with the charge-normalized interatomic distances within the complex, affirming and expanding existing predictive relationships, but also with the Debye−Waller parameter of the first coordination shell. The derived structure−activity relationships not only quantitatively relate the measured physical architecture of aqueous complexes to their observed stability but also allow for the prediction of siderophore−metal stability constants.

Introduction

In addition to Fe(III), siderophores form stable complexes with a number of contaminant metals (*1*−*8*), which may affect their sorption to mineral surfaces (*9*−*12*) and redox chemistry (*13*−*17*), and thus their ultimate fate and transport in the environment. Siderophores are a chemically diverse group of compounds, containing multidentate combinations of hydroxamate, carboxylate, and catecholate moieties (*18*); currently, approximately 500 different molecular structures classified as siderophores are known (*19*). The specificity of siderophores for different metal cations, as well as the stability of the resulting complexes, is closely linked to their structures. For desferrioxamine B (DFOB), a trihydroxamate siderophore produced by several species of *Streptomyces* (*20*), the terrestrial bacterium *Anthrobacter simplex* (*21*), and marine bacteria (*22, 23*), chelation of Fe(III) results in delocalization of electrons of the C=O and N−O$^-$ groups in the hydroxamate moieties that bind directly to the central metal ion, an effect that stabilizes the complex (*24, 25*).

The stability constants of metal−siderophore complexes are critical parameters for the accurate assessment of their effects on metal fate and transport, and an extensive database of these constants may lead to improved predictive geochemical models. To estimate these parameters, a correlation has been established between the log-transformed stability constant and both the log-transformed first hydrolysis constant (*6, 26*−*28*) and some form of the ionic potential or ionic force [e.g., z/IR (*27*) or $z/(4\pi \mathrm{IR}^2)$ (*29*)] of the complexed metal ion. Both types of correlation can be rationalized by noting that increased metal ion hardness results in increased coulomb interaction strength with the hard oxygen atoms in the hydroxamate moieties of DFOB; the second type of correlation also highlights the close relationship between chemical stability and molecular structure, although this correlation is based solely on the average properties of metal ions derived from crystallographic data for solid phases. To date, the molecular structures of only a few metal−DFOB complexes have been rigorously characterized as aqueous species (*16, 24, 25, 30*−*32*).

Understanding the coordination chemistry and stability of aqueous metal−siderophore complexes is essential to elucidating the factors that control their biological uptake by microbes. Ferric iron has traditionally been considered the exclusive target ion for siderophores, and its roles in Fe(III) solubilization (*33*) and uptake (*18*) have been recently reviewed; however, other metals may have stability constants that exceed Fe(III)'s binding constant (*16, 34*). In addition, microbial deficiencies of other metals (viz. Mo, V) may stimulate siderophore production and metal uptake via siderophore-mediated pathways (*35, 36*). Metals from siderophore complexes may enter microbial cells by several routes (*20, 37*−*39*), including (1) reduction and concomitant release of the metal center, (2) exchange of the metal from the siderophore to another high-affinity ligand, and (3) uptake of the intact complex. Although these uptake processes operate by different mechanisms, the fundamental factors that control uptake via these pathways are related to chemical stability and physical structure of the metal−siderophore complexes.

In this study, we examine the molecular architecture of aqueous metal−DFOB complexes using extended X-ray absorption fine structure (EXAFS) spectroscopy. Desferrioxamine B was chosen as the siderophore because the stability constants for a wide range of metal−DFOB complexes are known (*1, 2, 16, 19, 40*) and it is an environmentally widespread ligand, occurring in fresh (*41*) and marine waters (*22, 23*). The metals studied were chosen for their environmental importance as nutrients and/or contaminants (Cu, Zn, Mn, and Ni), or because of their useful role in the study of metal complexation chemistry (Ga). Direct measurement of the molecular architecture of these aqueous metal complexes allows for the exploration of quantitative structure−activity relationships (QSARs) that may further our fundamental understanding of metal−siderophore binding and serve as a predictive tool for estimating complex structure and stability.

Experimental Section

Materials. All solutions are made with deionized water with a resistivity of 18.3 MΩ·cm. Unless otherwise specified, all other chemicals are ACS reagent grade. The sample of

* To whom correspondence should be addressed.
† North Carolina State University.
‡ Stanford Synchrotron Radiation Lightsource.
§ University of California.

10.1021/es802044y CCC: $40.75
Published on Web 12/10/2008

DFOB utilized in this study is the mesylate salt $[(C_{25}H_{46}N_5O_8NH_3)^+(CH_3SO_3)^-]$ produced under the trade name Desferal. The sample is a gift from the Salutar Corp. The basic procedure for preparing solution containing $M^{n+}HDFOB^{n-2}$ complexes (50 mM) was the addition of the chloride salts [Cu(II), Ni(II), and Zn(II)] to a stoichometric concentration of DFOB dissolved in a small amount of water. The pH was set with addition of NaOH and HCl to values chosen to optimize the aqueous speciation (not shown) as the $M^{n+}HDFOB^{n-2}$ complex by using MINEQL+ (*42*) and published stability constants (Table 1 in Supporting Information) (*1, 2, 14, 16, 19*) corrected to the infinite dilution reference state with the Davies equation (*43*). However, the synthesis of Ga(III)$HDFOB^+$ and Mn(II)$HDFOB^0$ required modifications to the basic synthetic procedure. Because $Ga(III)Cl_3$ is a highly hydroscopic solid that decomposes upon exposure to air, a concentrated (0.56 M) solution was used to introduce the metal to the DFOB solution to form the Ga(III)$HDFOB^+$ complex. The Mn(II) complex was prepared as above, except the solution was prepared in a serum bottle with a continuous nitrogen purge to avoid air-oxidation of the complex (*14*). Attempts to produce Fe(II)$HDFOB^0$ in an anaerobic glovebox complexes were unsuccessful, most likely due to autoxidation (*15, 44*).

X-ray Spectroscopy of Metal−Hydroxamate Complexes. The metal K-edge EXAFS spectra of solutions (50 mM) containing Cu(II)$HDFOB^0$ at pH = 10.0, Ni(II)$HDFOB^0$ at pH = 9.0, Ga(III)$HDFOB^+$ at pH = 9.0, and Mn(II)$HDFOB^0$ at pH = 9.7 were measured at the Stanford Synchrotron Radiation Laboratory (SSRL) beamline 11-2 at room temperature with a Lytle detector in fluorescence mode. The Zn K-edge EXAFS spectrum of a 50 mM solution of Zn(II)$HDFOB^0$ at pH = 9.5 was collected at Advanced Light Source (ALS) beamline 10.3.2. Spectra of the model compounds [50 mM solutions $Cu(II)Cl_2$, Cu(II)EDTA, $Ni(II)Cl_2$, Ni(II)EDTA, $Ga(III)Cl_3$, and Ga(III)EDTA] were collected at SSRL beamline 2-3 at room temperature in transmission mode. Sample holders had a 2.5 mm wide and 30 mm long aperture covered with 0.0005-in.-thick Kapton tape.

Structural Modeling of EXAFS Spectra of Metal−Hydroxamate Complexes. Spectra were background-subtracted, splined, and fit in *R*-space (*45*) over the range R = 1−6 Å via the SIXPack interface (*46*), which makes use of the IFEFFIT engine (*47*). Amplitude and phase functions were derived from fitting spectral data by use of the FEFF6l code with single-scattering paths. The amplitude reduction factor (S_0^2) was fixed for all shells at 0.835 for Mn (*48*) and 0.86 for Zn (*49*), based on previous work by our group, and at 1.0 for Ga, 0.96 for Ni, and 0.90 for Cu, based on spectral fits for model compounds (results not shown). For each sample, the parameter ΔE_0 was allowed to float during optimization but was linked to a common value for all shells. Unless otherwise noted, the coordination number (N) was fixed for all shells based upon the physical model described below. Interatomic distances (R) were independently optimized for each shell; the Debye−Waller parameter (σ^2) was allowed to float during optimization and was independent for each shell. Uncertainty in optimized EXAFS parameters is reported as standard deviation, except for coordination number, which is assumed to be ±20% (*50*).

To fit the spectra of $M^{n+}HDFOB^{2-n}$ complexes, we employed a three-shell model based on the known structure of Fe(III)$HDFOB^+$ (*16, 30, 31*). The first shell represents the oxygen atoms directly coordinating the metal (Figure 1). For this shell, N was allowed to float freely, except for Cu(II) (see below).The second shell represents the carbon and nitrogen atoms contained in the hydroxamate moieties and is modeled as a single shell of six carbon atoms. A third shell, modeled as 25 carbon atoms, represents the average position of the atoms in the C/N backbone. Based on poor fits to an undistorted octahedron, this model was modified (*16*) to account for the Jahn−Teller axial Cu−O bond lengthening in Cu(II)$HDFOB^0$ (*51*) by splitting the first shell into two shells, containing two (axial) and four (equatorial) atoms; however, unlike the Mn(III)$HDFOB^+$ complex (*16*), the fit was not appreciably improved by splitting the second shell, and thus the Cu(II)$HDFOB^0$ spectrum was fit with a single second shell of six C atoms.

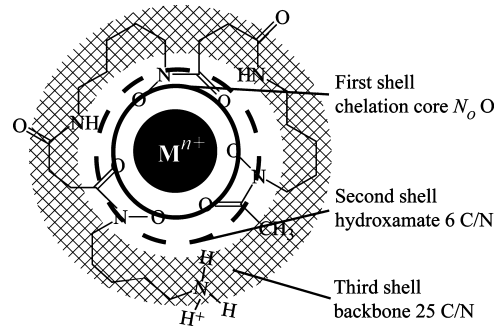

FIGURE 1. Structural basis for the modeling of EXAFS spectra of $M^{n+}HDFOB^{n-2}$ complexes. The distal oxygen atoms in the amide moieties of the backbone are not included in the model.

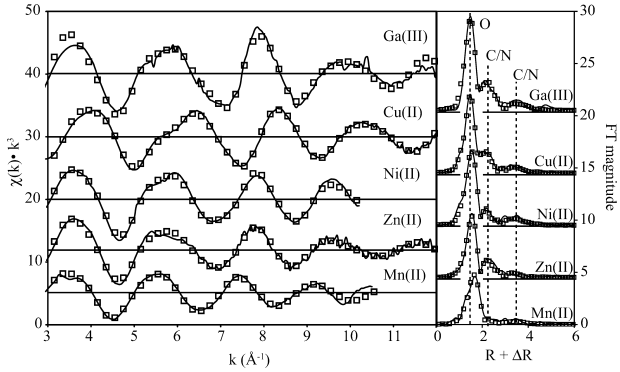

FIGURE 2. K-edge EXAFS spectra of Ga(III)$HDFOB^+$, Cu(II)$HDFOB^0$, Ni(II)$HDFOB^0$, Zn(II)$HDFOB^0$, and Mn(II)$HDFOB^0$. Solid lines indicate experimental data, while open points indicate the fit of a structural model. Optimized fitting parameters are shown in Table 1.

Results

Structure of Metal−Siderophore Complexes. Figure 2 shows the EXAFS spectra and Fourier transforms (FTs) of $M^{n+}HDFOB^{n-2}$ complexes. The FTs of all complexes show a large peak at $R + \Delta R$ near 1.6 Å, with smaller peaks appearing at longer distances. The first FT peak corresponds to the oxygen atoms coordinating to the central metal ion. The peaks at longer distances correspond to a second shell of C/N (ca. 2.1 Å $R + \Delta R$) associated with the hydroxamate groups and a third shell of C/N atoms (ca. 3.5 Å $R + \Delta R$) associated with the backbone of the molecule (*16, 30, 31*). Results of the model fits are shown in Table 1. The first-shell coordination number determined for each complex ($5.4 < N_O < 6.2$) is consistent with octahedral coordination, as previously established for several $M^{n+}HDFOB^{n-2}$ complexes (*16, 30−32*).

First- and second-shell interatomic distances agree well with those found in very similar metal complexes. First shell M−O distances for Ga(III)$HDFOB^+$ (1.976 ± 0.007 Å), Zn(II)$HDFOB^0$ (2.034 ± 0.006 Å), and Ni(II)$HDFOB^0$ (2.044 ± 0.005 Å) are in the range reported for corresponding solid-phase metal monohydroxamate complexes (1.970−1.974, 2.006−2.067, and 2.017−2.111 Å, respectively) (*52*). Additionally, there is good agreement between our first- and second-shell distances and those in related complexes. Gallium−oxygen bond distances in aqueous octahedral carboxylate complexes

TABLE 1. Amplitude Reduction Factors, Coordination Numbers, Interatomic Distances, and Debye–Waller Factors for $M^{n+}HDFOB^{n-2}$ Complexes Derived from EXAFS Fitting[a]

		first shell M–O			second shell M–C/N			third shell M–C/N		
metal	S_0^2	N_0	R_0 (Å)	σ_0^2 (Å^2)	$N_{C/N2}$[b]	$R_{C/N2}$ (Å)	$\sigma_{C/N2}^2$ (Å^2)	$N_{C/N3}$[b]	$R_{C/N3}$ (Å)	$\sigma_{C/N3}^2$ (Å^2)
Ni(II)	0.90	6.2	2.044[5]	0.0061[8]	6	2.81[2]	0.009[1]	25	4.42[3]	0.017[4]
Zn(II)	0.86 (*49*)	5.4	2.034[6]	0.0073[9]	6	2.83[1]	0.008[1]	25	4.48[6]	0.027[9]
Mn(II)	0.835 (*48*)	5.8	2.164[9]	0.008[1]	6	2.99[8]	0.03[1]	25	4.69[7]	0.03[1]
Ga(III)	1.0	6.0	1.976[7]	0.006[1]	6	2.80[2]	0.006[1]	25	4.47[5]	0.018[6]
Cu(II)	0.90	4[b,c]	1.920[4]	0.0038[3]	6	2.70[1]	0.007[1]	25	4.28[3]	0.020[4]
		2[b,c]	2.30[3]	0.017[5]						
Mn(III) (*16*)	0.835 (*48*)	4[b,c]	1.931[6]	0.0044[4]	4[c]	2.80[1]	0.0029[9]	25	4.35[6]	0.025[8]
		2[b,c]	2.19[2]	0.004[1]	2[c]	3.30[4]	0.005[4]			
Co(II) (*16*)	0.84 (*16*)	6.1	2.072[5]	0.0110[9]	6	2.87[2]	0.017[2]	25	4.57[4]	0.025[5]
Co(III) (*16*)	0.84 (*16*)	6[b]	1.884[3]	0.0029[4]	6	2.667[8]	0.0041[8]	25	4.19[4]	0.018[5]
Fe(III) (*16, 31*)	0.87 (*16*)	5.3	2.016[5]	0.0025[6]	6	2.840[9]	0.0022[8]	25	4.39[3]	0.013[4]
Fe(III) (*30*)	0.9 (*30*)	6.3	2.01[1]	0.007	5.4	2.84[1]	0.004	12.6	4.06[1]	
Cd(II) (*32*)		5.8	2.27[1]	0.0086	5.8	3.10[2]	0.0038			

[a] Numbers in brackets are experimental uncertainties in the last decimal place. Error in N is estimated as ±20% (*74*). [b] Fixed coordination number. [c] $N = 4$ and $N = 2$ represent oxygen atoms at equatorial and axial positions, respectively, of Jahn–Teller distorted complexes [e.g., Cu(II)HDFOB^0 and Mn(III)HDFOB$^+$]. Data for Co(II)HDFOB^0, Co(III)HDFOB$^+$, Mn(III)HDFOB$^+$, and Fe(III)HDFOB$^+$ are from Duckworth et al. (*16, 31*) and Edwards et al. (*30*). Data for Cd(II)HDFOB^0 are from Mishra et al. (*32*).

(1.95–2.05 Å) agree well with our first-shell M–O distances (*53, 54*). Our 2.80 ± 0.02 Å second-shell distance is close to the 2.73 Å distance seen for carbons in the five-membered rings of the aqueous Ga–citrate complex (*54*). For Ni(II)HDFOB^0, our first- and second-shell distances agree well with the 2.06 Å Ni–O and 2.85 Å Ni–C distances found for corresponding shells in aqueous octahedral Ni–organic acid and Ni–humic acid complexes (*55, 56*). For Mn(II)HDFOB^0, our first- and second-shell interatomic distances of 2.164 ± 0.009 and 2.99 ± 0.08 Å are in the range of corresponding distances (2.12–2.16 and 3.03–3.09 Å) reported for dissolved Mn(II) complexes with functionalized thiazolidine-4-carboxylic acids (*57*).

Deviations from Octahedral Coordination. Divalent copper commonly forms complexes with Jahn–Teller distorted octahedral coordination (*58*). To accommodate this distortion in our model for Cu(II)HDFOB^0, we split the first shell such that it contain two atoms in axial positions (ax) and four atoms in equatorial positions (eq) at independent distances. Our first-shell equatorial distances ($R_{eq} = 1.920 \pm 0.004$ Å) agree well with Cu in a number of solid and aqueous octahedral complexes (*59–64*). Axial O atoms are difficult to fit in EXAFS spectra and are often omitted from structural models (*64, 65*); indeed, $\sigma_{ax}^2 = 0.017$ Å^2 we determined is relatively large, indicating relatively large thermal and static disorder. Nonetheless, our axial Cu–O bond distance ($R_{ax} = 2.30 \pm 0.03$ Å) agrees well with reported Cu–O axial bond distances (*60, 62*). Second-shell equatorial Cu–C/N interatomic distance (2.70 ± 0.01 Å) are near those reported in the literature for related complexes in solution (*61, 62*).

Zinc is commonly found in multiple coordination states in the environment (*58*). Our first-shell M–O bond distance for Zn(II)HDFOB^0 (2.034 ± 0.007 Å) is considerably shorter than the Zn–O bond distances (2.07 Å) in hexaaquo–Zn and Zn–citrate complexes (*66, 67*) but longer than the Zn–O bond distances (1.96 Å) of tetrahedral $ZnO_{(s)}$ (*68*). Our bond distance, coupled with a somewhat low coordination number of 5.4, suggests that a fraction of the Zn(II) in our system may be in 5-fold, or possibly 4-fold, coordination (*69*). Although pH-dependent metal–siderophore speciation is often simple (*30*), recent work has uncovered a surprisingly complicated coordination chemistry for Pb(II) and DFOB (*32*), a system with stability constants similar to those of Zn(II) with DFOB (*2*). However, our data do not support an unambiguous quantitative decoupling of these complexes, which are generally consistent with the presence of Zn(II) complexes in 5- or 6-fold coordination or a mixture of complexes in 4-, 5-, and 6-fold coordination (*69*). Second-shell C/N distances are consistent with those found for complexes with ligands that form five-membered chelate rings with zinc (*66, 69, 70*).

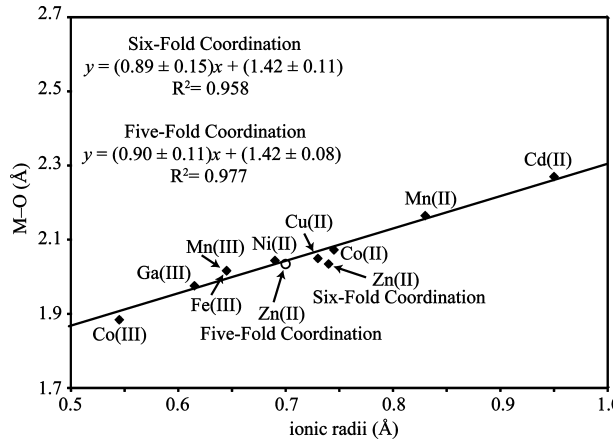

FIGURE 3. Average metal–oxygen bond distances versus ionic radii (*71*). A best-fit line is drawn for ionic radii in octahedral coordination (◆). When multiple electron configurations are accessible, all metals are assumed to be in the high-spin state except Co(III), which is believed to be in low-spin configuration in Co(III)HDFOB$^+$ (*16*). (○) Ionic radius of Zn(II) in 5-fold coordination. For Jahn–Teller distorted complexes [e.g., Cu(II)HDFOB^0 and Mn(III)HDFOB$^+$], average bond distances are coordination-number-weighted averages to account for complex distortion. Data for Co(II)HDFOB^0, Co(III)HDFOB$^+$, Mn(III)HDFOB$^+$, and Fe(III)HDFOB$^+$ are from Duckworth et al. (*16, 31*). Data for Cd(II)HDFOB^0 are from Mishra et al. (*32*).

Discussion

Metal–Oxygen First Coordination Shell. The number, distance, and denticity of M–O bonds at the chelation core are directly related to key geochemical properties of complexes, notably including stability. A plot (Figure 3) of the average metal–oxygen bond distance, from this and previous studies (*16, 31, 32*), versus the corresponding average metal ionic radius (Table 1 in Supporting Information) yields a linear relationship (*52*). Literature data for Pb(II) are excluded from this plot and from further analysis due to uncertainties in its speciation and coordination number (*32*). For

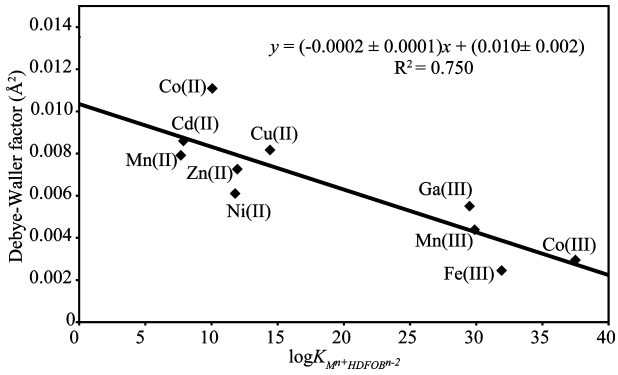

FIGURE 4. Plot of average first-shell Debye−Waller factor (σ^2) versus log $K_{M^{n+}HDFOB^{n-2}}$. Stability constants (*1, 2, 14, 16, 19*) are corrected to the infinite dilution reference state by use of the Davies equation (*43*). For Jahn−Teller distorted complexes [e.g., Cu(II)HDFOB^0 and Mn(III)HDFOB$^+$], Deybe−Waller factors are coordination-number-weighted averages to account for complex distortion. Dashed lines represent 95% confidence intervals. Data for Co(II)HDFOB^0, Co(III)HDFOB$^+$, Mn(III)HDFOB$^+$, and Fe(III)HDFOB$^+$ are from Duckworth et al. (*16, 31*). Data for Cd(II)HDFOB^0 are from Mishra et al. (*32*).

Jahn−Teller distorted complexes [viz. Mn(III)HDFOB$^+$ and Cu(II)HDFOB^0], average bond distance is defined as the coordination-number-weighted average of axial and equatorial bond distances [viz. $(2R_{ax} + 4R_{eq})/6$]. The best-fit regression line possesses a slope ($R^2 = 0.958$; $m = 0.89 \pm 0.15$) that is statistically equal to the expected slope of unity; furthermore, the *y*-intercept of 1.42 ± 0.11 Å is within error estimates of the reported ionic radius (1.35 Å) of doubly coordinated oxygen (*71*), which is the coordination environment oxygen atoms in the core of M^{x}HDFOB^{2-x} complexes (Figure 1). Interestingly, the correlation ($R^2 = 0.977$; $m = 0.90 \pm 0.11$; regression line not shown) is measurably improved if the ionic radius of Zn(II) in 5-fold coordination (Figure 3, ○) is utilized in the analysis instead of that of Zn(II) in octahedral coordination. This observation provides further permissive evidence that nonoctahedrally coordinated Zn(II)−DFOB complexes may be present in our sample.

Thermal and static disorder of the oxygen atoms in the first coordination shell is related to the complex stability constant. A negative correlation exists ($R^2 = 0.750$) between log $K_{M^{n+}HDFOB^{n-2}}$ for 10 metal complexes (Table 1 in Supporting Information) and the first-shell average Debye−Waller factor (σ_O^2), a measure of thermal and static disorder of the oxygen atoms around the metal center (Figure 4). (For Jahn−Teller distorted complexes [viz. Mn(III)HDFOB$^+$ and Cu(II)HDFOB^0], the average Debye−Waller factor is defined as the coordination-number-weighted average of σ_O^2 [viz. $(2\sigma_{ax}^2 + 4\sigma_{eq}^2)/6$].) This correlation suggests that the structural details of the first oxygen shell are important to the energetics of the complex.

To a first approximation, hard metal−oxygen bonds can be treated as harmonic oscillators with force constants being analogous to bond strength (*72*). Strong complexes are expected to have stronger electrostatic interactions between the hard oxygen atoms and charge-dense hard metal ions (viz. trivalent ions), and hence possess stronger bonds with significantly higher force constants. Consequently, these bonds are expected to have smaller amplitudes of vibration, and hence smaller thermal disorder contributions as compared to complexes containing softer metal ions (viz. divalent ions). This prediction is consistent with the general trend, as well as the segregation of trivalent and divalent metal complexes, observed in Figure 4. Crystallographic data suggest that static disorder may also contribute to the correlation in Figure 4. Crystallized Fe(III)−DFOB (*73*) and metal−hydroxamates (*52*) exhibit two distinct M−O bond

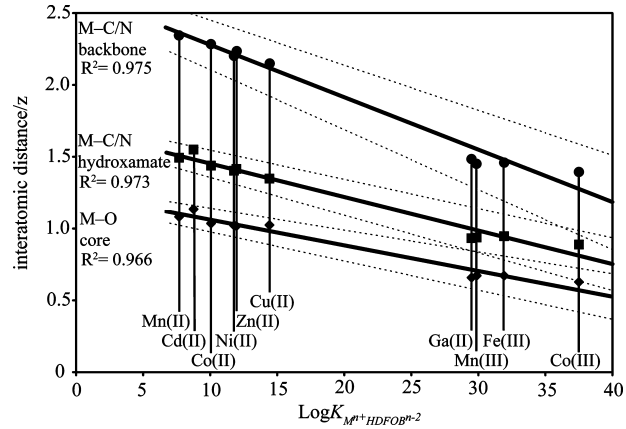

FIGURE 5. Plot of the average first-shell M−O (◆), second-shell M−C/N (■), and third-shell M−C/N (●) distances normalized by metal ion charge versus log $K_{M^{n+}HDFOB^{n-2}}$. Literature stability constants (*1, 2, 14, 16, 19*) are corrected to the infinite dilution reference state by use of the Davies equation (*43*). For Jahn−Teller distorted complexes [e.g., Cu(II)HDFOB^0 and Mn(III)HDFOB$^+$], average bond distances are coordination-number-weighted averages to account for complex distortion. Data for Co(II)HDFOB^0, Co(III)HDFOB$^+$, Mn(III)HDFOB$^+$, and Fe(III)HDFOB$^+$ are from Duckworth et al. (*16, 31*). Data for Cd(II)HDFOB^0 are from Mishra et al. (*32*). Dashed lines represent 95% confidence intervals. Vertical lines connect data points to labels specifying the complexed metal.

distances corresponding to the two distinct types of oxygen atom (viz. C=O and N−O$^-$) in the coordinating hydroxamate moieties of the first shell. The M−O(N) bonds are slightly shorter than M−O(C) bonds, mostly likely because of the negative charge on N−O$^-$ (as opposed to neutral C=O) in the dominant resonance structure of hydroxamate. Differences in the M−O(C) and M−O(N) bond lengths tend to increase with increasing metal ionic radius for hydroxamate complexes (*52*). Hence we expect that static disorder in the coordination core for M^{n+}HDFOB^{n-2} complexes should increase with bond distance (and thus log $K_{M^{n+}HDFOB^{n-2}}$; cf. Figure 5), which is also consistent with the trend observed in Figure 4. Our results thus suggest that small ionic radius and higher charge on the central metal cation favor more stable complexes with less disorder among the coordinating oxygen atoms at the complex core.

Quantitative Structure−Activity Relationships. The strengths of M−O bonds in the complex's core are directly related to complex stability (*24, 25*). Studies have shown a correlation between log $K_{M^{n+}HDFOB^{n-2}}$ and ionic potential (*z*/IR) (*27*). This type of correlation, which has been used in a slightly modified form [$z/(4\pi IR^2)$] to estimate metal binding constants for catechol and acetohydroxamic acid (*29*), is rationalized by noting that charge-dense hard metals with high ionic potentials interact strongly with the hard oxygen atoms in siderophore moieties. However, the ionic radii utilized in these relationships are based on bond distances derived from crystalline solids (*71*), not the aqueous complexes themselves, and thus neglect any of the specific effects of ligand−metal interactions on coordination chemistry. A similar correlation based on charge-normalized average metal−oxygen bond distances (M−O/*z*) measured in situ for aqueous DFOB complexes is shown as the bottom line in Figure 5. This correlation utilizes M−O/*z* as the independent variable instead of *z*/IR because the former is convenient for the comparison of stability constants with second- and third-shell interatomic distances, as discussed below.

Predictive relationships for the estimation of stability constants are most useful when based on widely available published data, such as tabulated ionic radii (*71*). In addition

to a comparison of bond distances to ionic radii (Figure 1), we compare correlation results based on the directly measured M—O bond distances from this study to correlations based on published ionic radii (Figure 1 in Supporting Information). The correlation coefficient for log $K_{M^{n+}HDFOB^{n-2}}$ plotted against our charge-normalized M—O bonds distances ($R^2 = 0.966$) is greater than that for a regression using the charge-normalized ionic radius ($R^2 = 0.918$), indicating that in situ measurements provide a more accurate assessment of the relationship between structure and stability. However, the similarity in correlation constants is useful in that it validates the use of published ionic radii for the estimation of $M^{n+}HDFOB^{n-2}$ stability constants. In addition, this study, coupled with previous work (*27, 29*), suggests that this type of correlation may be useful for other siderophores that have a sufficient number of known stability constants to support correlation analysis.

Additional structural parameters trend with the log *K* of $M^{n+}HDFOB^{n-2}$ complexes. The charge-normalized average M—C/N interatomic distances in both the hydroxamate moieties and the molecule's backbone correlate with log $K_{M^{n+}HDFOB^{n-2}}$ (Figure 5). Because there is no direct bonding between the metal center and C/N atoms, correlations based on interatomic distances cannot be rationalized in the same way as for M—O bonds. Instead, these relationships may indicate that changes in structure resulting from difference in metal size propagate through the complex. Moreover, the slopes of the best-fit regression lines for each shell increase with the distance of the shell from the metal center, suggesting that small changes in the coordination center at the core of the complex are indeed amplified in the surrounding shells, significantly affecting the overall size and structure of the complex. Understanding these systematic changes in structure with metal identity may be critical for elucidating the fundamental mechanism by which microbes select metal—siderophore complexes. Structural changes in the siderophore near the complex core have been known to alter uptake, and large differences have been noted in the uptake of different trivalent metal—siderophore complexes (*39*), highlighting the potential selective relationship between microbial receptors and metal—siderophore complexes.

The results of this study also help to elucidate the fundamental structural factors that control the stability of metal complexes with hexadentate ligands, including high-affinity biogenic chelating agents. Given the overwhelming structural diversity of siderophores (*19*), understanding which factors control metal binding and selectivity is critical to generalizing results from well-studied model systems (viz. DFOB) to the other environmentally relevant siderophores. In situ measurements reveal that $M^{n+}HDFOB^{n-2}$ complex stability is strongly correlated with interatomic distances, thus affirming, refining, and extending existing predictive relationships (*27*). In addition, correlations presented herein elucidate relationships between stability constants and both complex size and disorder. These correlations relate stability constants to structural parameters that may prove to be critical to understanding microbial metal uptake and other key aspects of environmental reactivity.

Acknowledgments

We are grateful to Kenneth Raymond for providing our sample of Desferal. We thank Edward Bellfield, Elena Pelen, Olivia Dong, Joe Rogers, Matthew Marcus, and Andrew Yang for logistical support and Jasquelin Peña, Kelley Roe, Brandy Toner, Dorothy Parker, Tom Spiro, Oyeyemi Oyerinde, and Andrzej Jarzecki for valuable discussion. We also acknowledge the thoughtful comments of Stephan Kraemer and two anonymous reviewers. This work was funded by the Kearney Foundation of Soil Science, University of California, and the National Science Foundation, Collaborative Research Activities in Environmental Molecular Science (CRAEMS) program (CHE-0089208). Portions of this research were carried out at the Stanford Synchrotron Radiation Lightsource, a national user facility operated by Stanford University on behalf of the U.S. Department of Energy, Office of Basic Energy Sciences. The SSRL Structural Molecular Biology Program is supported by the Department of Energy, Office of Biological and Environmental Research, and by the National Institutes of Health, National Center for Research Resources, Biomedical Technology Program. The Advanced Light Source is supported by the Director, Office of Science, Office of Basic Energy Sciences, of the U.S. Department of Energy under Contract DE-AC02-05CH11231.

Supporting Information Available

A figure comparing correlations between log $K_{M^{n+}HDFOB^{n-2}}$ and M—O/*z* and IR/*z*, as well as a table containing relevant stability constants and ionic radii. This material is available free of charge via the Internet at http://pubs.acs.org.

Literature Cited

(1) Anderegg, G.; L'Eplattenier; Schwarzenbach, G. Hydroxamatkomplexe II. Die anwendung der pH-methode. *Helv. Chim. Acta* **1963**, *46*, 1400–1408.
(2) Hernlem, B. J.; Vane, L. M.; Sayles, G. D. Stability constants for complexes of the siderophore desferrioxamine B with selected heavy metal cations. *Inorg. Chim. Acta* **1996**, *244*, 179–184.
(3) Whisenhunt, D. W.; Neu, M. P.; Hou, Z. G.; Xu, J.; Hoffman, D. C.; Raymond, K. N. Specific sequestering agents for the actinides. 29. *Inorg. Chem.* **1996**, *35*, 4128–4136.
(4) Frazier, S. W.; R., K.; Kraemer, S. M. Bacterial siderophores promote dissolution of UO_2 under reducing conditions. *Environ. Sci. Technol.* **2005**, *39*, 5709–5715.
(5) Brainard, J. R.; Strietelmeier, B. A.; Smith, P. H.; Langston-Unkefer, P. J.; Barr, M. E.; Ryan, R. R. Actinide binding and solubilization by microbial sideophores. *Radiochem. Acta* **1992**, *58*, 357–363.
(6) Jarvis, N. V.; Hancock, R. D. Some correlations involving the stability of complexes of transuranium metal ions and ligands with negatively charged oxygen donors. *Inorg. Chem. Acta* **1991**, *182*, 229–232.
(7) Wichard, T.; Bellenger, J. P.; Loison, A.; Kraepiel, A. M. L. Catechol siderophores control tungsten uptake and toxicity in the nitrogen-fixing bacterium *Azotobacter vinelandii*. *Environ. Sci. Technol.* **2008**, *42*, 2408–2413.
(8) Dahlheimer, S. R.; Neal, C. R.; Fein, J. B. Potential mobilization of platinum-group elements by siderophores in surface environments. *Environ. Sci. Technol.* **2007**, *41*, 870–875.
(9) Hepinstall, S. E.; Turner, B. F.; Maurice, P. A. Effects of siderophores on Pb and Cd adsorption to kaolinite. *Clays Clay Miner.* **2005**, *53*, 557–563.
(10) Kraemer, S. M.; Cheah, S. F.; Zapf, R.; Xu, J.; Raymond, K. N.; Sposito, G. Effect of hydroxamate siderophores on Fe release and Pb(II) adsorption by goethite. *Geochim. Cosmochim. Acta* **1999**, *63*, 3003–3008.
(11) Neubauer, U.; Nowack, B.; Furrer, G.; Schulin, R. Heavy metal sorption on clay minerals affected by the siderophore desferrioxamine B. *Environ. Sci. Technol.* **2000**, *34*, 2749–2755.
(12) Neubauer, U.; Furrer, G.; Schulin, R. Heavy metal sorption on soil minerals affected by the siderophore desferrioxamine B: the role of Fe(III) (hydr)oxides and dissolved Fe(III). *Soil Sci.* **2002**, *53*, 45–55.
(13) Dhungana, S.; Crumbliss, A. L. Coordination chemistry and redox processes in siderophore-mediated iron transport. *Geomicrobiol. J.* **2005**, *22*, 87–98.
(14) Duckworth, O. W.; Sposito, G. Siderophore—manganese(III) interactions I. Air-oxidation of manganese(II) promoted by desferrioxamine B. *Environ. Sci. Technol.* **2005**, *39*, 6037–6044.
(15) Kim, D.; Duckworth, O. W.; Strathmann, T. J. Hydroxamate siderophore-promoted reduction of nitroaromatic contaminants by iron(II) *Geochim. Cosmochim. Acta* **2008** (accepted for publication).
(16) Duckworth, O. W.; Jarzecki, A. A.; Bargar, J. R.; Spiro, T. G.; Sposito, G. An exceptionally stable cobalt(III)—desferrioxamine B complex *Mar. Chem.* **2008** (submitted for publication).
(17) Kazmi, S. A.; Shorter, A. L.; McArdle, J. V. Kinetics of reduction of ferrioxamine B by chromium(lI), vanadium(II), and dithionite. *J. Inorg. Biochem.* **1982**, *17*, 269–281.

(18) Winkelmann, G. Microbial siderophore-mediated transport. *Biochem. Soc. Trans.* 2002691–696.

(19) Kraemer, S. M.; Butler, A.; Borer, P.; Cervini-Silva, J. Siderophores and the dissolution of iron-bearing minerals in marine systems. In *Molecular Geomicrobiology*; Banfield, J. F., Cervini-Silva, J., Nealson, K. H., Eds.; Mineralogical Society of America: Chantilly, VA, 2005; Vol. 59, pp 53−84.

(20) Muller, G.; Raymond, K. N. Specificity and mechanism of ferrioxamine-mediated iron transport in *Streptomyces pilosus*. *J. Bacteriol.* **1984**, *160*, 304–312.

(21) Winkelmann, G., Specificity of iron transport in bacteria and fungi. In *CRC Handbook of Microbial Chelates*; Winkelmann, G., Ed.; CRC Press: Boca Raton, FL, 1991.

(22) McCormack, P.; Worsfold, P. J.; Gledhill, M. Separation and detection of siderophores produced by marine bacterioplankton using high-performance liquid chromatography with electrospray ionization mass spectrometry. *Anal. Chem.* **2003**, *75*, 2647–2652.

(23) Gledhill, M.; McCormack, P.; Ussher, S.; Achterbeg, E. P.; Mantoura, R. F. C.; Worsfold, P. J. Production of siderophore type chelates by mixed bacterioplankton populations in nutrient enriched seawater incubations. *Mar. Chem.* **2004**, *88*, 75–83.

(24) Edwards, D. C.; Myneni, S. C. B. Near edge X-ray absorption fine structure spectroscopy of bacterial hydroxamate siderophores in aqueous solutions. *J. Phys. Chem. A* **2006**, *110*, 11809–11818.

(25) Edwards, D. C.; Nielsen, S. B.; Jarzecki, A. J.; Spiro, T. G.; Myneni, S. C. B. Experimental and theoretical vibrational spectroscopy studies of acetohydroxamic acid and desferrioxamine B in aqueous solution: Effects of pH and iron complexation. *Geochim. Cosmochim. Acta* **2005**, *69*, 3237–3248.

(26) Evers, A.; Hancock, R. D.; Martell, A. E.; Motekaitis, R. J. Metal ion recognition in ligands with negatively charged oxygen donor groups. Complexation of Fe(III), Ga(III), In(III), Al(III) and other highly charged ions. *Inorg. Chem.* **1989**, *28*, 2189–2195.

(27) Hernlem, B. J.; Vane, L. M.; Sayles, G. D. The application of siderophores for metal recovery and waste remediation: Examination of correlations for prediction of metal affinities. *Water Resour.* **1999**, *33*, 951–960.

(28) Kiss, T.; Farkas, E. Metal-binding ability of desferrioxamine B. *J. Inclusion Phenom. Mol. Recognit. Chem.* **1998**, *32*, 385–403.

(29) Hider, R. C. Siderophore mediated absorption of iron. *Struct. Bonding (Berlin)* **1984**, *58*, 25–87.

(30) Edwards, D. C.; Myneni, S. C. B. Hard and soft X-ray adsorption spectroscopic investigations of aqueous Fe(III)−hydroxamate siderophore complexes. *J. Phys. Chem. A* **2005**, *109*, 10249–10256.

(31) Duckworth, O. W.; Bargar, J. R.; Sposito, G. Sorption of ferric iron from ferrioxamine B to synthetic and biogenic layer type manganese oxides. *Geochim. Cosmochim. Acta* **2008**, *72*, 3371–3380.

(32) Mishra, B.; Haack, E. A.; Vasconelos, I. F.; Maurice, P. A.; Bunker, B. A. XAFS determination of Pb and Cd speciation with siderophores and the metal/siderophore/kaolinate system. In *13th International Conference on X-ray Absorption Fine Structure (XAFS13)*; Hedman, B., Pianetta, P., Eds.; American Institute of Physics: Stanford, CA, 2006; pp 196−198.

(33) Kraemer, S. M. Iron oxide dissolution and solubility in the presence of siderophores. *Aquat. Sci.* **2004**, *66*, 3–18.

(34) Parker, D. L.; Sposito, G.; Tebo, B. M. Manganese(III) binding to a pyoverdine siderophore produced by a manganese(II)-oxidizing bacterium. *Geochim. Cosmochim. Acta* **2004**, *68*, 4809–4820.

(35) Liermann, L. J.; Guynn, R. L.; Anbar, A.; Brantley, S. L. Production of a molybdophore during metal-targeted dissolution of silicates by soil bacteria. *Chem. Geol.* **2005**, *220*, 285–302.

(36) Bellenger, J. P.; Wichard, T.; Kustka, A. B.; Kraepiel, A. M. L. Uptake of molybdenum and vanadium by a nitrogen-fixing soil bacterium using siderophores. *Nat. Geosci.* **2008**, *1*, 243–246.

(37) Leong, J.; Neilands, J. B. Mechanisms of siderophore iron transport in enteric bacteria. *J. Bacteriol.* **1976**, *126*, 823–830.

(38) Stintzi, A.; Barnes, C.; Xu, L.; Raymond, K. N. Microbial iron transport via a siderophore shuttle: A membrane ion transport paradigm. *Proc. Natl. Acad. Sci. U.S.A.* **2000**, *97*, 10691–10696.

(39) Ecker, D. J.; Loomis, L. D.; Cas, M. E.; Raymond, K. N. Coordination chemistry of microbial iron transport. 39. Substituted complexes of enterobactin and synthetic analogues as probes of the ferric enterobactin receptor in *Escherichia coli*. *J. Am. Chem. Soc.* **1988**, *110*, 2457–2464.

(40) Duckworth, O. W.; Sposito, G. Siderophore−manganese(III) interactions II. Manganite dissolution promoted by desferrioxamine B. *Environ. Sci. Technol.* **2005**, *39*, 6045–6051.

(41) Duckworth, O. W.; Holmstr̈om, S. J. M.; Peña, J.; Sposito, G. Biogeochemistry of iron oxidation in a circumneutral freshwater habitat *Chem. Geol.* **2008** (in press).

(42) Schecher, W. D.; McAvoy, D. C. MINEQL+: A Chemical Equilibrium Program for Personal Computers, Environmental Research Software: Hallowell, ME, 2001.

(43) Pankow, J. F. *Aquatic Chemistry Concepts*; CRC Press: Boca Raton, FL, 1991.

(44) Farkas, E.; Enyedy, E. A.; Fabian, I. New insight into the oxidation of Fe(II) by desferrioxamine B (DFB): spectrophotometric and capillary electrophoresis (CE) study. *Inorg. Chem. Commun.* **2003**, *6*, 131–134.

(45) Kelly, S. D.; Hesterberg, D.; Ravel, B. Analysis of soils and minerals using X-ray absorption spectroscopy. In *Methods of Soil Analysis*; Ulery, A. L., Drees, L. R., Eds.; Soil Science Society of America: Madison, WI, 2008.

(46) Webb, S. M. SIXPACK: A graphical user interface for XAS analysis using IFEFFIT. *Phys. Scr.* **2005**, 1011–1014.

(47) Newville, M. IFEFFIT: Interactive XAFS analysis and FEFF fitting. *J. Synchrotron Radiat.* **2001**, *8*, 322–324.

(48) Webb, S. M.; Tebo, B. M.; Bargar, J. R. Structural characterization of biogenic Mn oxides produced in seawater by the marine *Bacillus*sp. strain SG-1. *Am. Mineral.* **2005**, *90*, 1342–1357.

(49) Toner, B.; Manceau, A.; Webb, S. M.; Sposito, G. Zinc sorption to biogenic hexagonal-birnessite particles within a hydrated bacterial biofilm. *Geochim. Cosmochim. Acta* **2006**, *70*, 27–43.

(50) Brown, G. E., Spectroscopic studies of chemisorption reaction mechanisms at oxide-water interfaces. In *Mineral-Water Interface Geochemistry*; Hochella, M. F., White, A. F., Eds.; Mineralogical Society of America: Washington, DC, 1990; Vol. 23, pp 309−364.

(51) Jahn, H. A.; Teller, E. Stability of polyatomic molecules in degenerate electronic states. I. Orbital degeneracy. *Proc. R. Soc. London., A: Math. Phys. Sci* **1937**, *161*, 220–235.

(52) Codd, R. Traversing the coordination chemistry and chemical biology of hydroxamic acids. *Coord. Chem. Rev.* **2008**, *252*, 1387–1408.

(53) Clausen, M.; Ohman, L. O.; Persson, P. Spectroscopic studies of aqueous gallium(III) and aluminum(III) citrate complexes. *J. Inorg. Biochem.* **2005**, *99*, 716–726.

(54) Clausen, M.; Ohman, L. O.; Kubicki, J. D.; Persson, P. Characterisation of gallium(III)-acetate complexes in aqueous solution: A potentiometric, EXAFS, IR and molecular orbital modelling study. *J. Chem. Soc., Dalton Trans.* **2002**, 2559–2564.

(55) Nachtegaal, M.; Sparks, D. L. Nickel sequestration in a kaolinite−humic acid complex. *Environ. Sci. Technol.* **2003**, *37*, 529–534.

(56) Strathmann, T. J.; Myneni, S. C. B. Speciation of aqueous Ni(II)-carboxylate and Ni(II)-fulvic acid solutions: Combined ATR-FTIR and XAFS analysis. *Geochim. Cosmochim. Acta* **2004**, *68*, 3441–3458.

(57) Nagy, L.; Yamaguchi, T.; Yamashita, S.; Nomura, M.; Gajda, T.; Buzas, N.; Wakita, H. EXAFS and XANES studies of Ni(II), Zn(II), Mn(II) and Ag(I) complexes of some 2-(polyhydroxyalkyl)thiazolidine-4-carboxylic acids. *ACH−Models Chem.* **2000**, *137*, 1–23.

(58) Cotton, F. A.; Wilkinson, G.; Murrillo, C.; Bochmann, M. *Advanced Inorganic Chemistry*; Wiley: New York, 1999.

(59) Brown, G. M.; Chidamba, R. Dinuclear copper(II) acetate monohydrate - Redetermination of structure by neutron-diffraction analysis. *Acta Crystallogr., Sect. B: Struct. Sci.* **1973**, *29*, 2393–2403.

(60) Korshin, G. V.; Frenkel, A. I.; Stern, E. A. EXAFS study of the inner shell structure in copper(II) complexes with humic substances. *Environ. Sci. Technol.* **1998**, *32*, 2699–2705.

(61) Karlsson, T.; Persson, P.; Skyllberg, U. Complexation of copper(II) in organic soils and in dissolved organic matter - EXAFS evidence for chelate ring structures. *Environ. Sci. Technol.* **2006**, *40*, 2623–2628.

(62) Nagy, L.; Yamaguchi, T.; Nomura, M.; Ohtaki, H. EXAFS and XANES studies of Cu(II) complexes formed with adenosine or uridine at different hydrogen ion concentrations. *ACH−Models Chem.* **2000**, *137*, 575–589.

(63) Lee, Y. J.; Elzinga, E. J.; Reeder, R. J. Cu(II) adsorption at the calcite-water interface in the presence of natural organic matter: kinetic studies and molecular-scale characterization. *Geochim. Cosmochim. Acta* **2005**, *69*, 49–61.

(64) Sheals, J.; Persson, P.; Hedman, B. IR and EXAFS spectroscopic studies of glyphosate protonation and copper(II) complexes of glyphosate in aqueous solution. *Inorg. Chem.* **2001**, *40*, 4302–4309.
(65) Cheah, S. F.; Brown, G. E.; Parks, G. A. XAFS study of Cu model compounds and Cu^{2+} sorption products on amorphous SiO_2, γ-Al_2O_3, and anatase. *Am. Mineral.* **2000**, *85*, 118–132.
(66) Karlsson, T.; Skyllberg, U. Complexation of zinc in organic soils - EXAFS evidence for sulfur associations. *Environ. Sci. Technol.* **2007**, *41*, 119–124.
(67) Kelly, R. A.; Andrews, J. C.; DeWitt, J. G. An X-ray absorption spectroscopic investigation of the nature of the zinc complex accumulated in *Datura innoxia* plant tissue culture. *Microchem. J.* **2002**, *71*, 231–245.
(68) Bochatay, L.; Persson, P. Metal ion coordination at the water−manganite (g-MnOOH) interface. II. An EXAFS study of zinc(II). *J. Colloid Interface Sci.* **2000**, *229*, 593–599.
(69) Sarret, G.; Manceau, A.; Spadini, L.; Roux, J. C.; Hazemann, J. L.; Soldo, Y.; Eybert-Berard, L.; Menthonnex, J. J. Structural determination of Zn and Pb binding sites in *Penicillium chrysogenum* cell walls by EXAFS spectroscopy. *Environ. Sci. Technol.* **1998**, *32*, 1648–1655.
(70) Harding, M. M. The geometry of metal−ligand interactions relevant to proteins. *Acta Crystallogr., Sect. D: Biol. Crystallogr.* **1999**, *55*, 1432–1443.
(71) Shannon, R. Revised effective ionic radii and systematic studies of interatomic distances in halides and chalcogenides. *Acta Crystallogr.* **1976**, *A32*, 751–767.
(72) Diem, M. *Introduction to Modern Vibrational Spectroscopy*; Wiley: New York, 1993; p 285.
(73) Dhungana, S.; White, P. S.; Crumbliss, A. L. Crystal structure of ferrioxamine B: a comparative analysis and implications for molecular recognition. *J. Biol. Inorg. Chem.* **2001**, *6*, 810–818.
(74) Brown, G. E.; Sturchio, N. C. An overview of synchrotron radiation applications to low temperature geochemistry and environmental science. In *Application of Synchrotron Radiation in Low-Temprature Geochemistry and Environmental Science*; Fenter, P., Rivers, M., Sturchio, N. C., Sutton, S., Eds.; Mineralogical Society of America: Washington, DC, 2002.

ES802044Y